

Study of Transient Temperature Distribution in a Friction Welding Process and its effects on its Joints.

Sirajuddin Elyas Khany¹, K.N.Krishnan², Mohd Abdul Wahed³

¹Associate Professor, ²Professor, ³Graduate Student,
MED, MJCET, Hyderabad, India.

Abstract:

In Materials like Stainless Steel 304 and Eutectoid Steel, microstructure is affected during the process of friction welding leading to variation in Hardness and strength. In the present Study, the transient temperature distribution in a friction welded Joint of similar materials in one dimension (uniaxial direction) is studied. A numerical method based on thermal networking is used to estimate the transient temperature distribution. Microstructure variation of specimen is also studied. The preliminary predictions are compared to actual experimental data from welding conducted under identical conditions. The results are shown to be in fair agreement. The numerical method proposed in this work provides guidance in weld parameter development and allows better understanding of the friction welding process.

Key Words: Friction Welding, Numerical Method, Temperature Distribution, Microstructure and Hardness.

Introduction:

In the present study, the friction welding technology used is one in which the rotational motion of the work pieces is stopped after the pressure has been applied for a very short period of time. During the process, the frictional heat is generated in the interface till plastic deformation stage is reached. Then, the rotation is stopped to let the welded joint cool down under free convection.

Peak joint temperature and the temperature profile in the region near the joint have a significant impact on the flash formation, the extend of heat effected zones and the joint strength. The thermal effects of the friction welding are observed to have lowered the hardness of the welded materials compared to the parent materials. Heating and cooling rates are closely related to the joint temperature and directly influence the residual stresses developed in the joint. Therefore, it is vital to have a means of rapidly and accurately estimating the peak joint temperature and cooling rates based on input parameters. A numerical method is developed, simulating the friction welding to quickly visualize the process specific responses to define the quality of the weld. An analysis of these phenomena is helpful in improving both the method and strength of the bonds in the welding process.

Mechanical evaluation and thermal modeling of friction welding of mild steel and aluminium is described by Hazman Seli et al (1). A new friction law of modeling of continuous drive friction welding and application to 1045 steel welds is presented by Balsubramaniam et al (2). Thermically evaluation and modeling of friction welding is presented by Ahmet Can et al (3). Estimation of heat generation at the interface of cylindrical bars during friction process is presented by Wen-lih Chen et al (4). Experimental and numerical analysis of the friction welding process for the 4340 steel and mild steel combinations is described by Akbari Mousavi et al (5). Numerical simulation of linear friction welding of titanium alloy: Effects of processing parameters is presented by Wen-ya li et al (6). Thermo-mechanical and diffusion modeling in the process of ceramic-metal friction welding is done by Jolanta Zimmerman et al (7). Dynamic simulation of the temperature field of stainless steel laser welding is described by Han GuoMing et al (8). Temperature and stress distribution in ultrasonic metal welding—An FEA-based study is presented by S. Elangovan et al (9).

The focus of the present paper is to understand the thermal effects on the weld work piece and analyze the transient temperature profiles in the welded rods during friction welding. The numerical method is applied in obtaining the solution and the resulting temperature fields are compared with experimental data.

Materials and Method:

A continuous drive friction welding as shown in fig. 1 was used to produce a weld between stainless steel- stainless steel and eutectoid steel- eutectoid steel rods of diameter 15mm and length 80mm.

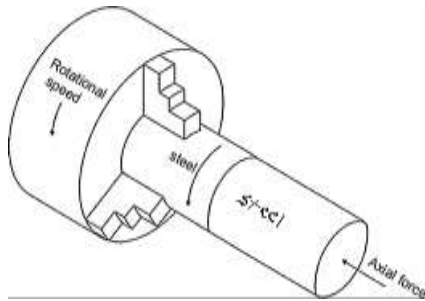


Fig. 1 Scheme of continuous drive friction welding

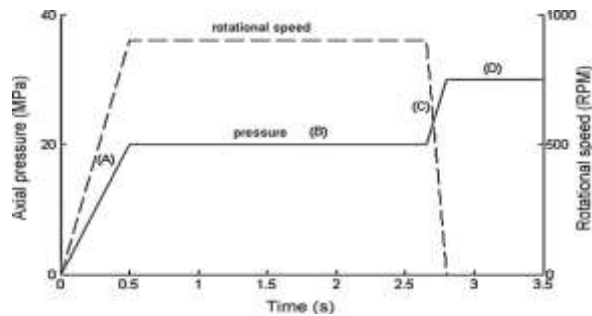


Fig. 2. Axial pressure and rotational velocity used in the experiment.

The changes of load and rotational speed in time during the process are shown in Fig. 2. The characteristic phases are marked. In phase (A), axial load and rotational speed of the steel rod were applied and the two rods were brought near the joined surfaces. Then in phase (B), the two rods underwent friction heating at the interface. When the rotational speed was stopped in phase (C), the frictional heated surface cooled down and at the same time, the upsetting under increased pressure occurred. Finally in phase (D), the pressure remained constant until the axial pressure is released.

The chemical composition of the Stainless steel and Eutectoid Steel employed in this study are summarized in Table 1. The temperature changes during the friction welding process are measured at a time by two k-type thermocouples attached to the stationary rod at a distance of 7mm, 14mm, 21mm and 28mm from the interface. The axial pressure is applied from the fixed end gradually. The temperature profiles are recorded at specific time intervals, till the welding is complete. The locations of the thermocouple is shown in fig.3.



Fig. 3. The locations of the thermocouple placement 7, 14, 21 and 24mm from the interface, respectively.

For metallurgical examination the welded sample is sectioned perpendicular to the weld interface. The joint sample is ground and polished. Microstructure is obtained using optical microscope. The Rockwell hardness is measured at the point of highest temperature from the interface (i.e. at 7mm from the interface).

Table 1 (Chemical composition of stainless steel 304 and eutectoid steel by wt %)

Element	C	Mn	P	Cu	Mo	S	Cr	N	Si	Fe	Ni
S.S(304)	0.08	20	0.045	0.75	0.75	0.05	20	0.10	1.00	Bal	10.5
Eutectoid steel	0.80	0.7	0.04	-----	-----	0.05	-----	-----	-----	-----	-----

3. Mathematical Modeling:

3.1. General assumptions for the analysis of friction welding:

- Heat generation and pressure across the interface are assumed to be uniform.
- There is no heat exchange between the end faces of the steel rods and the environment.
- The steel rods are assumed to be homogenous and isotropic.
- The heat input is considered constant throughout the process.

3.2. Thermal analysis:

During friction welding, the temperature in the weld region rises sharply due to extreme frictional heat and plastic deformation of the steel rod within a very short time. To calculate the temperature profile, the heat transfer analysis is undertaken by considering the frictional heat generation at the interface and heat loss to the surroundings by conduction and convection.

3.2.1. Frictional heat generation model:

Based on the assumption that force distribution remains constant, the frictional heat is deduced through the following analytical method.

First, a micro annulus with an inner radius r and a width dr in the friction surface is defined as in Fig. 4.

The constant pressure acting on the entire surface is given by p . The area of the micro annulus is $dA = (2\pi r) dr$. Transforming the pressure equation into a differential characterization of the area dA , the following equation is obtained for the differential force, dF , acting on the area dA .

$$dF = p dA = 2\pi p r dr \quad (1)$$

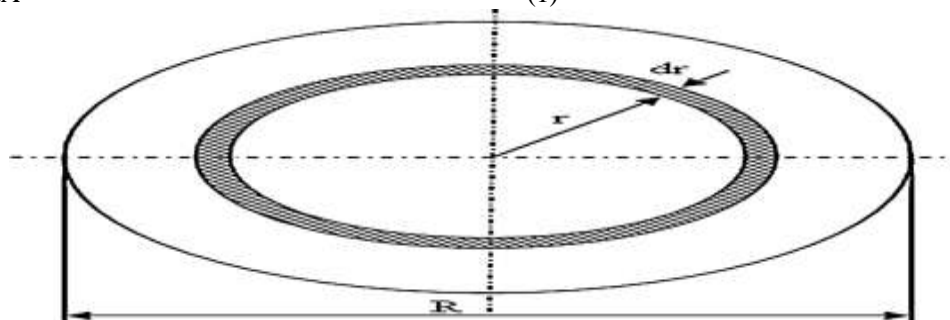


Fig. 4. Friction interface sketch.

Since dF is equivalent to the equal and opposite normal force acting on dA , the differential frictional force, dF_f , can be specified as

$$dF_f = \mu dF = 2\mu p r dr \quad (2)$$

Where μ is friction coefficient. It is known that the tangential velocity, v_T at any point on the element is the same,

$$v_T = r \omega \quad (3)$$

Where ω is angular velocity.

The differential power that is exerted to rotate the annulus area dA is

$$dP = dF_f (v_T) = 2\mu p r^2 \omega dr \quad (4)$$

Therefore, by integrating Eq. (4) with respect to r , the definition for the frictional heating power generation is obtained as

$$P = \int_0^R 2\mu p r^2 \omega dr = (2/3) \mu p \omega R^3 \quad (5)$$

The heat flux (q) generated by friction at the annulus is given as

$$q(r) = dP/dA = 1.6\mu p\omega r \quad (6)$$

3.3. Heat transfer:

The fundamental non-steady equation of Fourier's heat conduction in the coupled thermo-mechanical problem can be expressed as follows:

$$\partial T/\partial t + u (\partial T/\partial x) = 1/\rho C_p \partial/\partial x (k\partial T/\partial x) - hP/\rho C_p A (T - T_o) + q \quad (7)$$

where T is temperature, T_o is the ambient temperature around the rod, u is the shortening velocity, ρ is the material density, C_p is the specific heat capacity, A is the cross-sectional area, P is the perimeter of the rod, k is the thermal conductivity, h is the convection coefficient, x is the distance from the weld interface and t is time. For simplicity, Eq. (7) can be rewritten as

$$\partial T/\partial t + u (\partial T/\partial x) = \alpha (\partial^2 T/\partial x^2) - \beta (T - T_o) + q \quad (8)$$

Where $\alpha = k/\rho C_p$ and $\beta = hP/\rho C_p A$.

In this one-dimensional equation, the convection term on the right-hand side of the equation accounts for heat conduction and heat lost through convection along the lateral surfaces of the two components. It is assumed that there is no heat lost through radiation at the frictional interface. The problem of heat conduction in the whole process of friction welding determined by means of Eq. (8) was, thus, simplified to the calculation of temperature field, $T = T(x,t)$. The calculation of the temperature of the friction welding process is carried out in two stages. The first stage is the heating part while the second is the cooling process. The initial and boundary conditions when solving Eq. (8) are expressed based on the two stages.

3.3.1. Heating stage:

The temperature distribution is calculated for heating separately for the rod of length(L) by assuming common average heat generated at the interface. For the heating stage, the initial and boundary conditions for the simplified equation (8) are derived as

$$T(x, t_h) = T_o, \text{ for } t_h = 0 \quad (9)$$

$$-k (\partial T/\partial x) = q, x = 0 \text{ for } t_h > 0 \quad \text{and} \quad (10)$$

$$-k (\partial T/\partial x) = h (T - T_o), x = L, \text{ for } t_h > 0 \quad (11)$$

Where t_h is the heating or frictional time, T_o is the initial temperature of the specimen, q is the surface heat flux generated at the friction surface (x = 0).

3.3.2. Cooling stage (welded):

At this stage the rods have been joined and considered as one new rod for the calculation, where the initial and boundary conditions for the simplified equation (8) are derived as

$$T(x_j, t_c) = T_n, \text{ for } t_c = 0 \quad \text{and} \quad (12)$$

$$K_s (\partial T/\partial x) = h_a (T_s - T_o), x_j = 0, \text{ for } t_c > 0 \quad (13)$$

Where x_j is the distance from left end of the joined rods, t_c is the cooling time, k is the thermal conductivity of the steel, and T is the temperatures of the free surfaces of the steel. T_n is the last temperature profile from the previous heating stage. The only unknown in the equation presented above is the shortening velocity (u) which is assumed to be zero. The calculation of the temperature is carried out using FORTRAN.

The properties of Stainless steel 304 and Eutectoid steel are listed in Table 2. As shown below.

Properties	Stainless steel 304	Eutectoid steel
Density(kg/m ³)	7900	7840
Thermal conductivity(w/mk)	15	46
Specific heat(j/kg k)	477	470
Melting Point	1371 - 1532	°C

4. Results and discussion:

The experimental study is done on a continuous drive friction welding machine. The friction welding parameters were 490 and 790rpm rotational speed, 5-8 bar friction pressure and 11-15 bar upsetting pressure. Hardness profiles of parent and welded samples are determined. A one-dimensional numerical model for temperature profiles of this process is proposed and solved using FORTRAN program developed in the data processing center of Muffakham – Jah – College of Engg. & Tech. Hyderabad

4.1 Microstructure Variation:

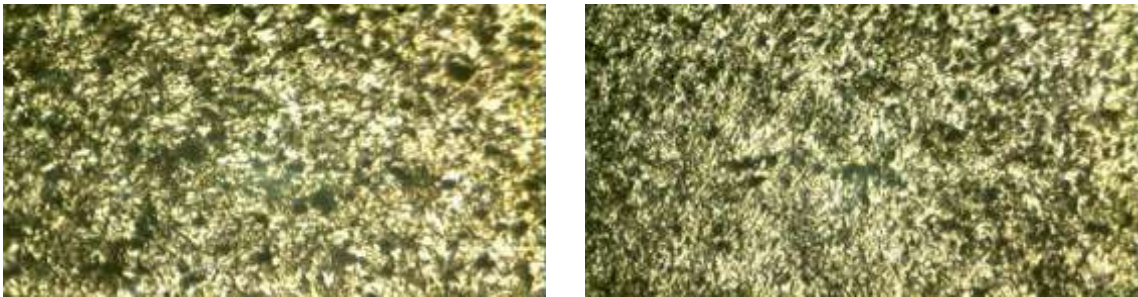


Fig.5 Microstructure variation of S.S 304 before and after friction welding at 675x.

The microstructure consists of single phase austenite. The microstructure is completely austenite of equiaxed uniform grains within the grains, slip bands are seen and the grain boundaries are clear. Precipitate of alloy carbides is noticed. Due to chemical composition deposition alloy carbides are seen which are not refined before friction welding.

Subjected to friction welding at 613°C (i.e. at a distance of 7mm, the highest peak temperature from the interface) it is observed that there is grain refinement along with the precipitation of carbides.

Before friction welding	After friction welding
Grain size ASTM: 6	Grain size ASTM: 7



Fig.6 Microstructure variation of Eutectoid steel before and after friction welding at 675x.

Microstructure reveals 100% pearlite in the form of lamella structure (alternate bands of cementite and ferrite) before friction welding. Dark areas are pearlite and light areas are ferrite.

Microstructure reveals 100% pearlite which is more refined after friction welding and can be seen in the form of lamella structure (alternate bands of cementite and ferrite).

In this study the highest temperature reached is 600°C (i.e. at a distance of 7mm from the weld interface) in both the steel rods. More changes in the microstructure are not expected because the temperature is within the range of eutectoid temperature (i.e. below 723°C).

4.2 Hardness Profile:

Fig. 7a and 7b shows the result of the Rockwell hardness test for S.S 304 and Eutectoid steel. The hardness value is checked for both the steel rods at distance of 7, 14, 21 and 28mm of welded part and is found to be lower at the first node (i.e. at 7mm) than that of its parent part. This reduction could be due to the thermal effect in the welded steel. Due to normalizing the hardness is increasing as the distance from the weld is increasing. In stainless steel 304, hardness is increasing gradually and in eutectoid steel rapidly this, difference in both the steel rods is due to the refinement of grain structure and homogenization of the microstructure due to normalizing.

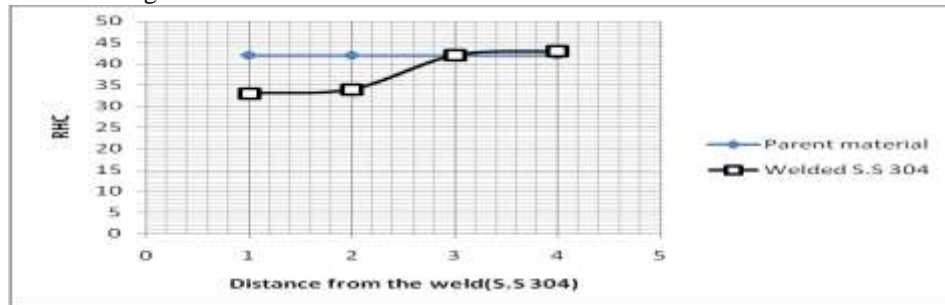


Fig.7a Results of the Rockwell hardness test for Stainless steel 304

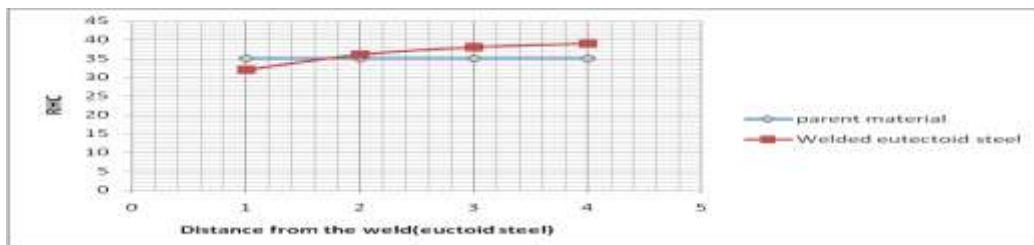


Fig.7b Results of the Rockwell hardness test for Eutectoid steel.

Due to normalizing, hardness is increasing in both the steel rods, and as the hardness is increases, strength also increases.

4.3 Heating and cooling stage:

The transient heating and cooling temperature distribution for steel rods are shown in Fig. (9a – 9p). From the temperature distribution, it is seen that the calculated peak temperature in heating for stainless steel at 90sec and 40sec is about 613°C and 378°C and for eutectoid steel is 578°C and 270°C at 200sec and 70sec, peak temperatures in heating for steel rods are obtained at a distance of 7mm from the interface at 490 and 790rpm with constant heat generated. Cooling starts of as the entire process, where the last heating temperature profile has been utilized. Similarly transient heating and cooling temperatures are obtained for similar parameters at 14, 21 and 28mm from the interface. The temperature increases rapidly at the interface, and gradually towards the end of the steel rods. The transient heating and cooling temperature distribution in eutectoid steel is faster. This is due to the higher thermal conductivity in eutectoid steel compared to that in stainless steel. Due to the lower thermal conductivity stainless steel is taking less time for welding when compared to eutectoid steel. As the speed (rpm) is increasing temperature as well as time is decreasing in both the steel rods, but the variation is nearly similar. The difference can be attributed to accomodating the heat losses at the interface in the analytical model.

The thermal heating profile likely exhibits the interaction between the frictional heating power and the frictional characteristics on the surface. However, in a real situation, the pressure distribution is not uniform with time as the two work pieces move in sinusoidal fashion. While the axial force remains constant, the area of contact between the two work pieces changes with movement and leads to the oscillation of the axial pressure at the interface. Therefore, altering the axial pressure during every cycle owing to the variation of contact area causes the frictional heat input to fluctuate as well. The friction coefficient varies widely with temperature. The increase in the temperature softens the ductile material and brings about deep ploughing on the contact surfaces. Then, the contact seems to have been altered into a polishing-like action and the friction coefficient is dramatically reduced. The inaccuracy in the calculation was attributed to the assumption of constant coefficient of friction and pressure for the analytical constant heat generation.

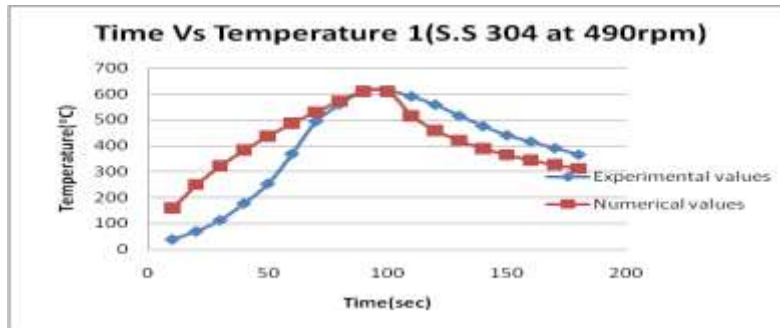


Fig.9a Time–temperature profiles at a distance of 7mm from the weld interface for numerical and experimental data of stainless steel at 490rpm.

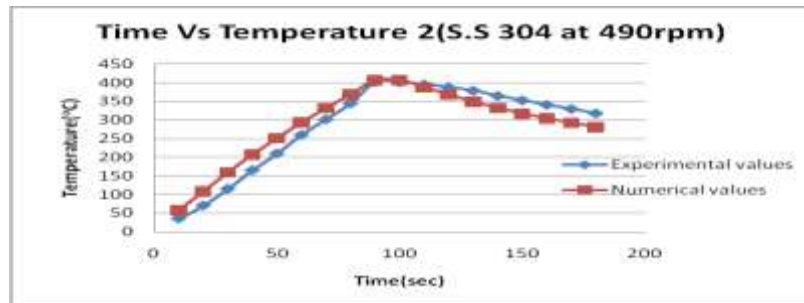


Fig.9b Time–temperature profiles at a distance of 14mm from the weld interface for numerical and experimental data of stainless steel at 490rpm

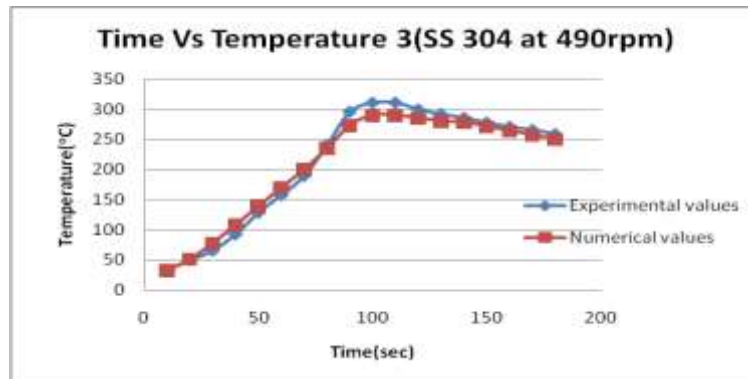


Fig.9c Time–temperature profiles at a distance of 21mm from the weld interface for numerical and experimental data of stainless steel at 490rpm

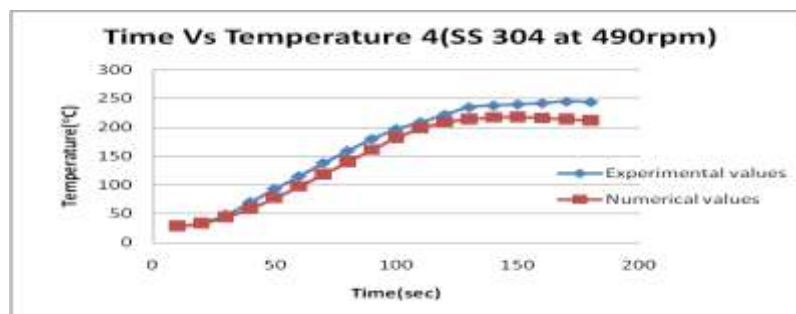


Fig.9d Time–temperature profiles at a distance of 28mm from the weld interface for numerical and experimental data of stainless steel at 490rpm

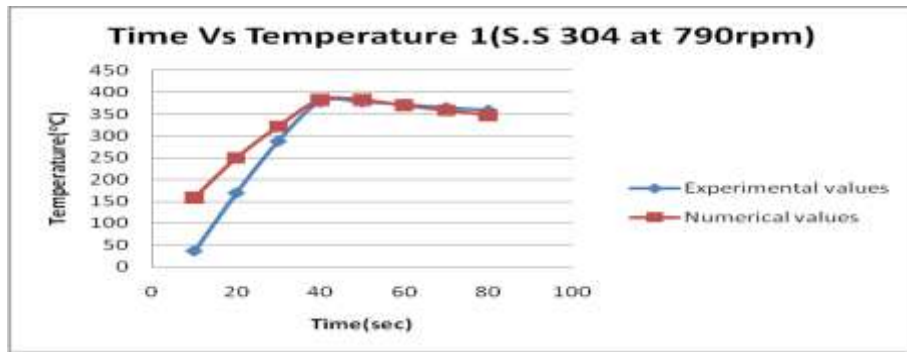


Fig.9e Time–temperature profiles at a distance of 7mm from the weld interface for numerical and experimental data of stainless steel at 790rpm

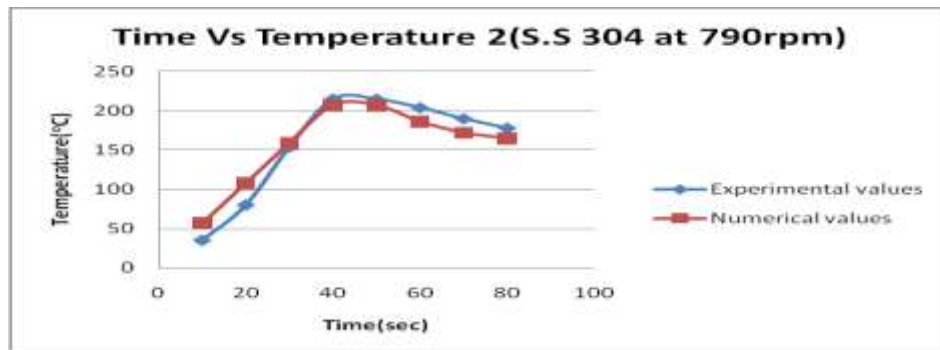


Fig.9f Time–temperature profiles at a distance of 14mm from the weld interface for numerical and experimental data of stainless steel at 790rpm

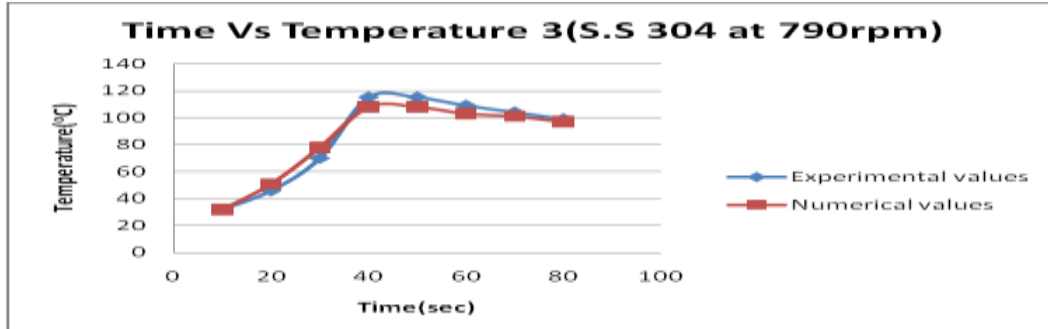


Fig.9g Time–temperature profiles at a distance of 21mm from the weld interface for numerical and experimental data of stainless steel at 790rpm

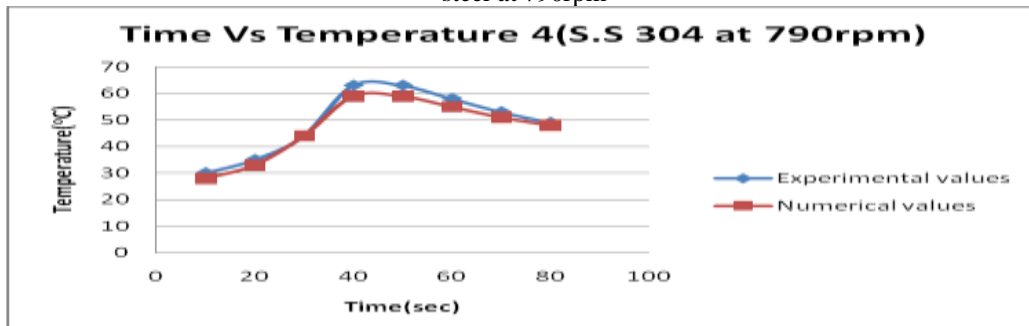


Fig.9h Time–temperature profiles at a distance of 28mm from the weld interface for numerical and experimental data of stainless steel at 790rpm

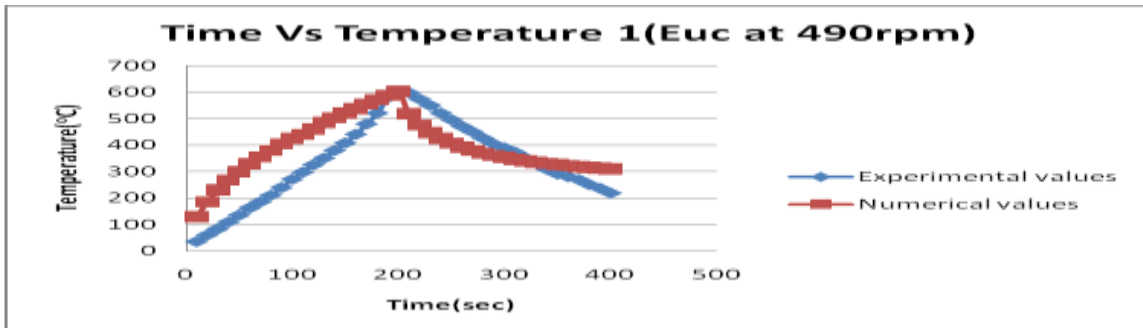


Fig.9i Time–temperature profiles at a distance of 7mm from the weld interface for numerical and experimental data of eutectoid steel at 490rpm

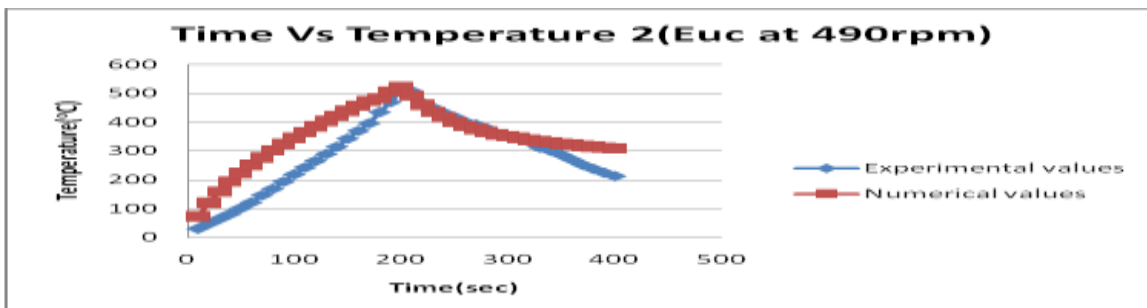


Fig.9j Time–temperature profiles at a distance of 14mm from the weld interface for numerical and experimental data of eutectoid steel at 490rpm

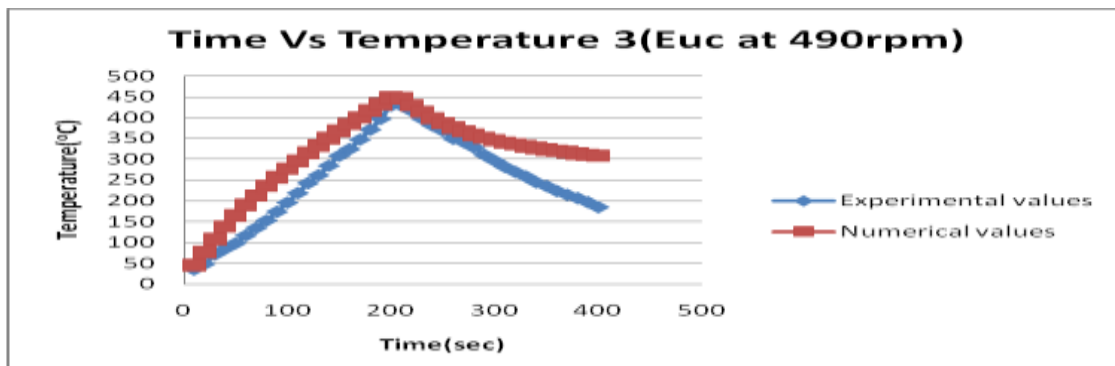


Fig.9k Time–temperature profiles at a distance of 21mm from the weld interface for numerical and experimental data of eutectoid steel at 490rpm

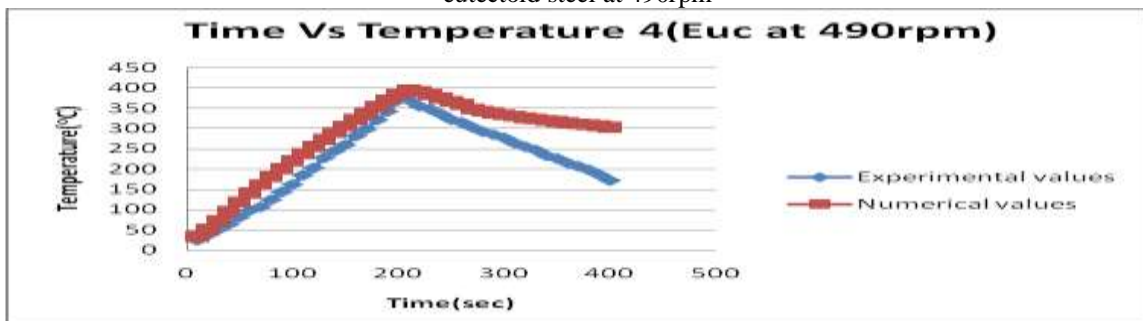


Fig.9l Time–temperature profiles at a distance of 28mm from the weld interface for numerical and experimental data of eutectoid steel at 490rpm

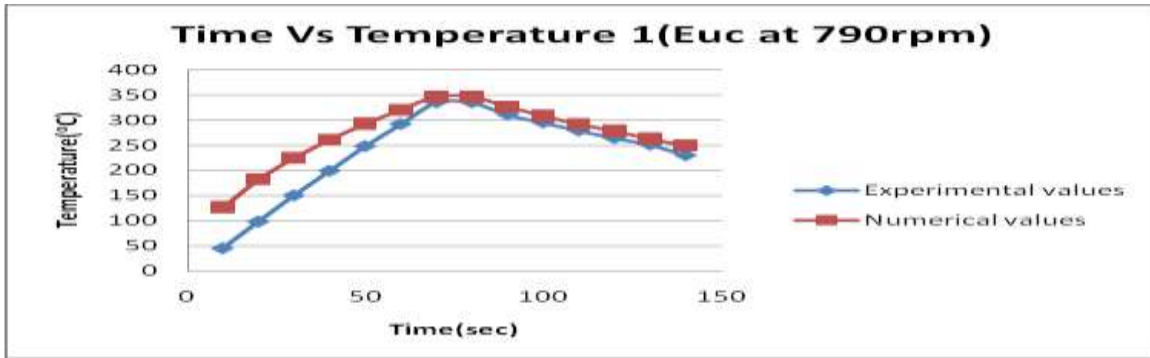


Fig.9m Time–temperature profiles at a distance of 7mm from the weld interface for numerical and experimental data of eutectoid steel at 790rpm

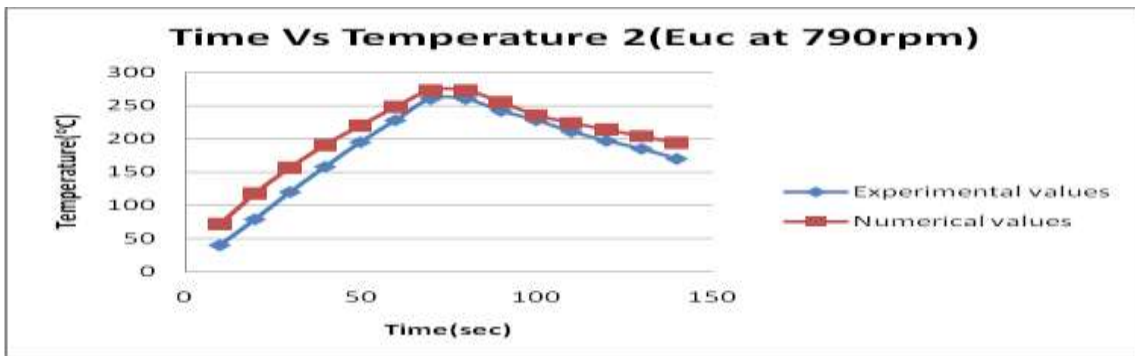


Fig.9n Time–temperature profiles at a distance of 14mm from the weld interface for numerical and experimental data of eutectoid steel at 790rpm

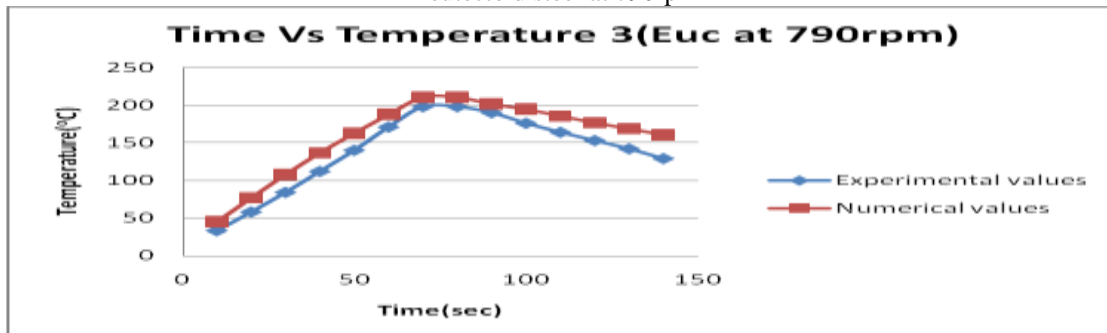


Fig.9o Time–temperature profiles at a distance of 21mm from the weld interface for numerical and experimental data of eutectoid steel at 790rpm

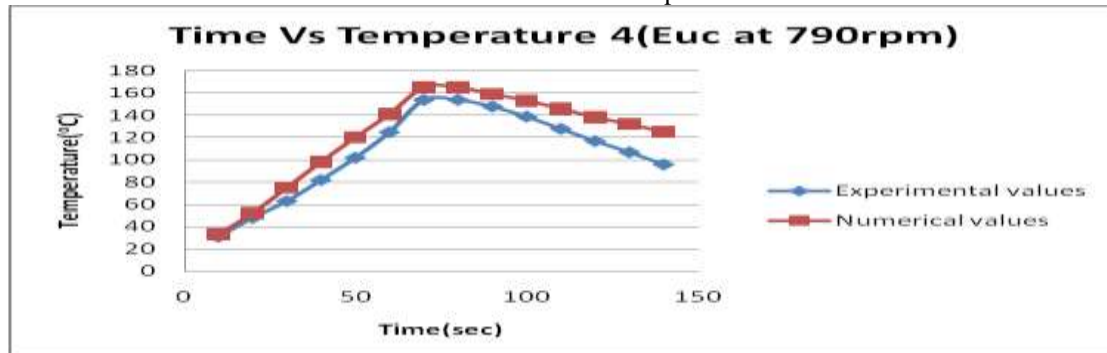


Fig.9p Time–temperature profiles at a distance of 28mm from the weld interface for numerical and experimental data of eutectoid steel at 790rpm

4.4. Verification of the predicted profile with experimental data:

The verification of the predicted temperature distribution of the welded rods are presented in Fig.9. for locations 7, 14, 21 and 28mm from the interface. The computed temperature profile does not exactly match with the experimental data. However, the trend of the profiles shown is similar.

The predicted heating and cooling temperature profiles of the friction welding are in fair agreement with the experimental temperature profiles. The heating and cooling rates of the process are approximately calculated around 138 °C/s and 45 °C/s, respectively. After the rotation of the steel rod is stopped, the temperature profile increases and decreases with lower gradients compared to the measured temperature profile. The discrepancy of the two temperature profiles is mostly attributed to the static nature of the model. After 10 s, the difference is quite significant, most probably because the proposed model does not consider the entire work pieces for calculation. In the friction welding process, at every moment of the friction phase, the plasticized material is expelled out of the faying surface due to the mutual movement of the mating surfaces. In contrast, the numerical model is simply based on the static analysis in which the heat generated at the interface is assumed to be totally transferred to the base materials with no flash formed (zero axial shortening assumption). Therefore, the relative movement (rubbing) of the two parts, which is the main reason for ejecting softened material from the rubbing surface, is not considered in the model. Apart from that, the errors could also come from the temperature measurement since operation is manual. Even though inaccurate, these details are still useful in friction welding process study, especially in explaining the heat affected zone which eventually affects the strength of the joint. Hence, the proposed model provides some parameter development and allows better understanding of the friction welding process.

5. Conclusions:

Bonds of stainless steel vs stainless steel and eutectoid steel vs eutectoid steel are achieved in the friction welding process. The welded materials have lower hardness measured at a distance of 7mm from the interface compared to their parent materials due to thermal effects of the friction welding. But as the distance from the interface is increasing hardness is increasing due to normalizing and this has been also compared with CCT diagram. A one-dimensional numerical model for continuous drive friction welding was developed according to the characteristics of the friction welding process. It is introduced to enable a better understanding of the process. The predicted transient heating and cooling temperature profile of the friction welding is in fair agreement with the experimental temperature distribution.

Acknowledgements:

The authors gratefully acknowledge the co-operation and help extended by Mr. Mansur from metal cutting laboratory and Mr. Hashmi from metallurgy laboratory in carrying out the experiment during this research work.

References:

- [1.] Hazman Seli, Ahmad Izani Md.Ismail, Endri Rachman, Zainal Arifin Ahmad.(2010) Mechanical evaluation & thermal modeling of friction welding of mild steel & aluminium. Journal of materials processing technology 210 (1209-1216).
- [2.] Vikram Balasubramaniana; Youlin Lib; Tim Stotlerc; Jeff Cromptonc; Alfred Soboyejoa; Noriko Katsubea; Wolé Soboyejo.(1999). A New Friction Law for the Modelling of Continuous Drive Friction Welding: Applications to 1045 Steel Welds, materials & manufacturing process, 14:6, (845-860).
- [3.] ahmet CAN, Mumin SAHIN & Mahmut KUCUK(2009).Thermically Evaluation & modeling of friction welding, strojarstvo 51(1) (5-13).
- [4.] Wen-lih chen, Yu-ching yang, Shao-shu chu(2009).Estimation of heat generation at the interface of cylindrical bars during friction process), Applied thermal Engineering 29 (351-357).
- [5.] s.a.a.akbari mousavi & a. rahbar kelishami(2008), Experimental & numerical analysis of the friction welding process for the 4340 steel & mild steel combinations. Welding research 178-186s(vol.87).
- [6.] Wen-ya li, Tiejun Ma, Jinglong Li(2010), Numerical simulation of linear friction welding of titanium alloy: Effects of processing parameters, Materials & Design 31(1497-1507).
- [7.] Jolanta Zimmerman, wladyslaw wlosinski, zdzislaw R Lindemann Thermo-mechanical & diffusion modeling in the process of ceramic-metal friction welding(2009), Journal of materials processing Technology 209, (1644-1653).
- [8.] Han GuoMing *, Zhao Jian, Li JianQang(2007), Dynamic simulation of the temperature field of stainless steel laser welding, Material & Design 28 (240-245).
- [9.] S. Elangovan, S. Semeer, K. Prakasan Temperature and stress distribution in ultrasonic metal welding—An FEA-based study (2009), Journal of material processing Technology 209,(1143–1150).